Two-temperature momentum distribution in a thulium magneto-optical trap

E. Kalganova,[1,*] O. Prudnikov,[2,3] G. Vishnyakova,[1,4] A. Golovizin,[1,4] D. Tregubov,[1,4] D. Sukachev,[1,5] K. Khabarova,[1,4] V. Sorokin,[1,4] and N. Kolachevsky[1,4]

[1]*P. N. Lebedev Physical Institute, Leninsky prospekt 53, 119991 Moscow, Russia*

[2]*Institute of Laser Physics, Siberian Branch, Russian Academy of Sciences, Prospekt Akademika Lavrentyeva 13/3, 630090 Novosibirsk, Russia*

[3]*Department of Physics, Novosibirsk State University, Pirogova St. 2, 630090 Novosibirsk, Russia*

[4]*Russian Quantum Center, Novaya St. 100A, Skolkovo, 143025 Moscow, Russia*

[5]*Department of Physics, Harvard University, Oxford St. 17, Cambridge, Massachusetts 02138, USA*

(Received 21 July 2017; published 29 September 2017)

Second-stage laser cooling of thulium atoms at the 530.7 nm transition with a natural linewidth of 350 kHz offers an interesting possibility to study different regimes of a magneto-optical trap (MOT). The intermediate value of the spectral linewidth of the cooling transition allows the observation of three distinct regimes depending on the intensity and detuning of the cooling beams, namely, the "bowl-shaped" regime when light pressure force competes with gravity, the "double structure" regime with interplay between the Doppler and polarization-gradient (sub-Doppler) cooling, and the "symmetric" regime when Doppler cooling dominates over sub-Doppler cooling and gravity. The polarization-gradient cooling manifests itself by a two-temperature momentum distribution of atoms resulting in a double-structure of the spatial MOT profile consisting of a cold central fraction surrounded by a hot halo. We studied the double structure regime at different saturation parameters and compared observations with calculations based on semiclassical and quantum approaches. The quantum treatment adequately reproduces experimental results if the MOT magnetic field is properly taken into account.

DOI: 10.1103/PhysRevA.96.033418

I. INTRODUCTION

Since the first demonstration of laser cooling of erbium atoms in 2006 [1], the interest in ultracold hollow-shell lanthanides is continuing to grow. In addition to the relative simplicity of laser cooling and availability of laser sources, most of these atoms possess a large ground-state magnetic dipole moment which makes them promising candidates for studies of long-range anisotropic interactions [2]. Recent advances in the preparation and control of laser-cooled ensembles of Dy [3], Er [4], Tm [5,6], and Ho [7] provide access to the physics of dipolar quantum gases [8,9], low-field Feshbach resonances [10], and quantum simulations of unexplored many-body phenomena [11]. Inner-shell transitions in lanthanides can also be used for optical frequency metrology [12,13].

Deep laser cooling of lanthanides in a magneto-optical trap (MOT) is often done in two steps. For Zeeman slowing and the first-stage MOT, a strong transition lying in the blue spectral range around 400 nm is typically used [1,7,14,15]. That allows one to reach temperatures around 100 μK. Lower temperatures are achieved using a second-stage MOT operating on a spectrally narrow or intermediate transition [16]. Two-stage laser cooling of the hollow-shell lanthanides was successfully demonstrated in Er [17], Dy [3], and Tm [5]. After the second stage cooling, atoms are loaded into an optical dipole trap or in an optical lattice for further studies.

For nearly all transitions involved in laser cooling of hollow-shell lanthanides, the magnetic Landé g factors of the upper and lower cooling levels are close to each other [18,19]. As a result, efficient sub-Doppler cooling was observed directly in the first-stage MOT of Tm [20], Dy [21], Er [22], and Ho [7] even in the presence of a strong magnetic field gradient. However, sub-Doppler cooling in the second-stage MOT has not been reported yet.

For the second-stage laser cooling of Tm atoms we use the transition at 530.7 nm with a natural spectral linewidth of $\Gamma = 2\pi \times 350$ kHz (Fig. 1). The intermediate transition linewidth and a small difference of magnetic Landé g factors allows us to observe competition between Doppler and sub-Doppler cooling as well as the interplay of gravity and light pressure force directly in the MOT. Depending on the saturation parameter S, we can observe three distinct regimes: the regular "symmetric" regime dominated by Doppler cooling, the "bowl-shaped" regime with the strong influence of gravity on MOT performance, and the most unusual "double structure" regime where Doppler and sub-Doppler cooling mechanisms compete. To describe the double structure regime we used semiclassical [23] and quantum [24,25] simulations of the cooling process. The quantum approach takes into account recoil effects and, contrary to semiclassical approach, adequately reproduces the momentum distribution in the cloud.

In this manuscript, we describe three MOT regimes and present experimental data (Sec. II). Section III shows results of the semiclassical and quantum treatments and a comparison with the experiment. Some conclusions are summarized in Sec. IV.

II. MOT REGIMES

We observe all three MOT regimes introduced in Sec. I by varying the saturation parameter $S = S_0/(1 + 4\Delta^2/\Gamma^2)$. Here $S_0 = I/I_{\text{sat}}$ is the saturation parameter on the exact resonance with I being the on-axis single-beam intensity and I_{sat} being the saturation intensity. The saturation intensity is defined as $I_{\text{sat}} = 2\pi^2 c\hbar\Gamma/3\lambda^3$, where λ is the wavelength of light, c is the speed of light, $\hbar$ is the reduced Planck constant, and Γ is the natural linewidth. For the second-stage Tm cooling transition

*kalganova.elena@gmail.com

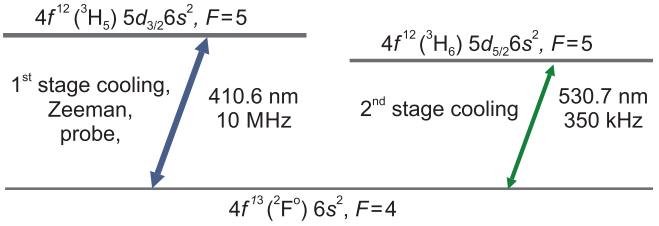

FIG. 1. Relevant energy levels of thulium. The strong transition at 410.6 nm is used for the first-stage laser cooling, the Zeeman slowing, and the imaging; the weak transition at 530.7 nm is used for the second-stage cooling.

$I_{\rm sat} = 0.32$ mW/cm^2. The detuning of the laser frequency ω from the atomic resonance frequency ω_0 is denoted as $\Delta = \omega - \omega_0$.

We use the conventional MOT configuration with three orthogonal pairs of circularly polarized cooling beams (the vertical beams are aligned with gravity). During the first cooling stage, atoms are trapped using both blue (410.6) and green (530.7 nm) cooling radiation simultaneously (Fig. 1). Then radiation at 410.6 nm (Zeeman and first-stage MOT cooling light) is blocked and atoms are further cooled only by 530.7 nm light for $\tau_{\rm sc} = 80$ ms (the second-stage MOT). After the second-stage cooling and a period of ballistic expansion, the cloud is imaged on a CCD-camera using a short pulse of resonant 410.6 nm light. More details about the experimental configuration are given in [5]. To study different MOT regimes, we perform several experiments with significantly different intensities and detunings of 530.7 nm light.

We measure that the second-stage MOT reaches a steady state faster than in 40 ms for the whole range of parameters used in this work which agrees with the theoretical estimations based on Ref. [26]. Accordingly, we choose the duration of the second-stage cooling (τ_{sc}) to be longer than 40 ms. This assures that the first-stage cooling only determines number of atoms trapped in the second-stage MOT but does not affect its dynamics.

Since the magnetic field gradients are different for horizontal and vertical directions (the anti-Helmholtz coils are axially aligned along the vertical axis z), the vertical and horizontal momentum distributions are also expected to be different. Henceforth, we will discuss momentum distribution and the corresponding temperature only for the vertical coordinate z (along gravity). Momentum distribution and temperature for the horizontal coordinates qualitatively demonstrate the same behavior and further discussion is valid for the horizontal coordinates as well.

Unlike in the broad-line MOT, the intermediate and narrow-line MOT operation can be dramatically affected by gravitational force and the recoil effect. The boundaries between three aforementioned regimes are roughly given by the following criteria for the saturation parameter S. The first criteria is the balance between the light pressure force and the gravitational force:

$$\frac{RS_0}{1 + S_0 + 4(\Delta/\Gamma)^2} = 1, \tag{1}$$

where $R = \hbar k\Gamma/2mg$. Here k is the wave vector of the cooling light, m is the atomic mass, and g is the free fall acceleration.

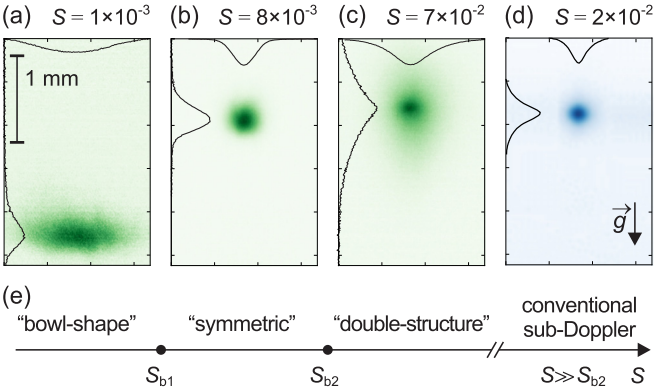

FIG. 2. (a)–(c) Images of the second-stage MOT cloud for (a) the bowl-shaped regime with $\Delta = -7\Gamma, S_0 = 0.1$; (b) the symmetric regime, $\Delta = -2.4\Gamma$, $S_0 = 0.1$; and (c) the double structure regime, $\Delta = -11\Gamma$, $S_0 = 37$. (d) Image of the first-stage MOT cloud for the conventional sub-Doppler regime with $\Delta = -1\Gamma$, $S_0 = 0.1$. The density profiles for vertical and horizontal axes are shown; g denotes the direction of the gravity. (e) MOT regimes depending on the saturation parameter value. The boundaries are $S_{\rm b1} = 2 \times 10^{-3}$, $S_{\rm b2} = 10^{-2}$ for the second-stage MOT [(a)–(c)] and $S_{\rm b1} = 5 \times 10^{-5}$, $S_{\rm b2} = 7 \times 10^{-4}$ for the first-stage MOT (d).

Thus, the first boundary saturation parameter value is

$$S_{\rm b1} = 1/(R - 1). \tag{2}$$

In our case $R = 500$ and the first boundary is $S_{\rm b1} = 2 \times 10^{-3}$.

The second boundary corresponds to the case when the width of the polarization-gradient force resonance in momentum domain [23]

$$\delta p = \frac{2m}{k} S\Gamma \tag{3}$$

becomes equal to the recoil momentum $\hbar k$:

$$S_{\rm b2} = \frac{\hbar k^2}{2m\Gamma}. \tag{4}$$

Thus, the second boundary equals $S_{\rm b2} = 10^{-2}$.

The MOT regimes and corresponding atomic cloud density profiles recorded in our experiments are depicted in Figs. 2(a) to 2(c) and are described further in more detail.

A. The bowl-shaped regime

When $S < S_{\rm b1}$, the light pressure force becomes comparable or smaller than the gravitational force. The cloud moves down to the region of nonzero magnetic field, reaching the equilibrium position on the surface where the Zeeman shift compensates for the light frequency detuning. At this surface, the light pressure force balances the gravitational force.

This causes three interesting effects. First, the cloud acquires a specific shape (the bowl-shape) as shown in Fig. 2(a). Second, the combined detuning becomes independent of the light frequency detuning Δ. As a consequence, the cloud temperature also becomes independent of Δ [Fig. 3(a)]. Third, atoms interact mostly with the upward propagating beam and become optically pumped to the lowest magnetic sublevel m_F, where F is the total atomic angular momentum. We verify atomic spin-polarization using the Stern-Gerlach experiment

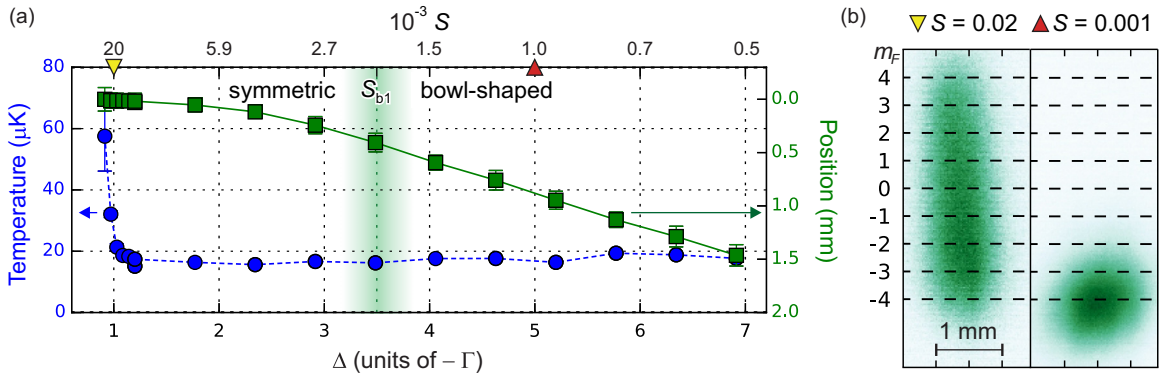

FIG. 3. (a) The MOT temperature (blue circles) and the position (green squares) of the cloud center vs the laser frequency detuning Δ in units of the minus natural linewidth $-\Gamma$. The resonant saturation parameter $S_0 = 0.1$. The respective values of detuning-dependent saturation parameters S are given on the top axis. One can distinguish the symmetric (detuning $|\Delta| < 3.5\Gamma$) and the bowl-shaped (detuning $|\Delta| > 3.5\Gamma$) regimes. The green vertical boundary shows the case when the saturation parameter S reaches S_{b1}. The lines are guidelines for the eye. (b) The Stern-Gerlach experiment. The cloud image is taken after 6 ms of ballistic expansion in a magnetic field with a gradient of 0.4 T/m. All magnetic sublevels m_F are well populated in the symmetric MOT regime (left, $S = 0.02$), while for the bowl-shaped regime, strong optical pumping to the $m_F = -4$ sublevel is observed (right, $S = 0.001$). Respective saturation parameter values are marked by the yellow downward triangle and the red upward triangle on the panel (a).

[Fig. 3(b)], switching off the MOT fields and applying a vertical magnetic field gradient of about 0.4 T/m. The optical pumping allows for the preparation of a spin-polarized atomic ensemble which is advantageous for further study of cold collisions.

This cooling regime was previously reported for Sr [16], Dy [27], and Er [17], and was analyzed in detail in [27,28].

B. The symmetric regime

If $S < S_{b2}$, the width of the polarization-gradient resonance in the momentum domain [Eq. (3)] is small compared to the recoil shift. As a result each photon scattering event pushes the atom out of the polarization-gradient resonance. In this case the polarization-gradient cooling mechanism (sub-Doppler cooling) does not play a significant role and only Doppler cooling takes place.

The interval

$$S_{b1} < S < S_{b2}$$

corresponds to the MOT regime with the Doppler cooling mechanism playing the dominant role when the light pressure force is much stronger than the gravity. In this case, the atomic cloud has a symmetric elliptical shape [Fig. 2(b)] which we refer to as the symmetric regime.

The symmetric ($S_{b1} < S < S_{b2}$) and the bowl-shaped ($S < S_{b1}$) regimes were observed for the cooling light intensities of 0.02–0.1 mW/cm^2 per beam ($S_0 = 0.06$–0.3) and detunings Δ in the range from -1Γ to -7Γ. Figure 3(a) shows the dependence of the atomic cloud temperature T on the frequency detuning Δ for $S_0 = 0.1$ and illustrates a transition between these two regimes.

C. The double-structure regime

If $S > S_{b2}$, δp becomes larger than the recoil momentum $\hbar k$. The polarization-gradient cooling starts impacting some fraction of an atomic ensemble, while the rest of the atomic cloud still possesses the momentum distribution determined by the Doppler cooling. As a result, the momentum distribution of the atomic ensemble becomes significantly different from the Maxwellian one, consisting of sub-Doppler and Doppler fractions (see Sec. III). In the harmonic potential, this results in a two-component spatial density distribution [Fig. 2(c)], which can be adequately approximated by the sum of two Gaussian functions.

We observe such cloud shapes for intensities higher than 3 mW/cm^2 ($S_0 > 9$) and for frequency detunings Δ from -4Γ to -12Γ. The ballistic expansion experiments show that the cloud consists of two atomic subensembles possessing different temperatures. There is a fraction of cold atoms which corresponds to a small central volume, and a hot fraction forming a spread halo. To determine temperatures of these two subensembles, the cloud density profiles obtained during ballistic expansion are fitted by the two Gaussian functions with independent parameters. The fit gives us the temperature of the sub-Doppler fraction T_{SD}, the temperature of the Doppler fraction T_D, as well as the relative number η of the sub-Doppler cooled atoms.

We observe the transition from the symmetric to the double structure regime by changing the 530.7 nm light intensity I ($S_0 \propto I$) at fixed Δ. Similar behavior can be observed by varying Δ at constant S_0. The corresponding temperatures T_D and T_{SD} are shown in Fig. 4. The fraction of the sub-Doppler cooled atoms η (shown in the same plots) grows for larger saturation parameters S. One can interpret this as the result of the sub-Doppler resonance broadening [Eq. (3)] which enhances the sub-Doppler cooling efficiency.

It is interesting to note that the temperature T_{SD} decreases with increasing light intensity; the effect is clearly visible for saturation parameters S in the range from 0.05 to 0.2. This is unusual for conventional pictures of sub-Doppler [23] and Doppler cooling [26], where the increase of cooling intensity always results in the increase of the temperature of atoms. The observed behavior is interpreted in the next section using the framework of MOT quantum theory.

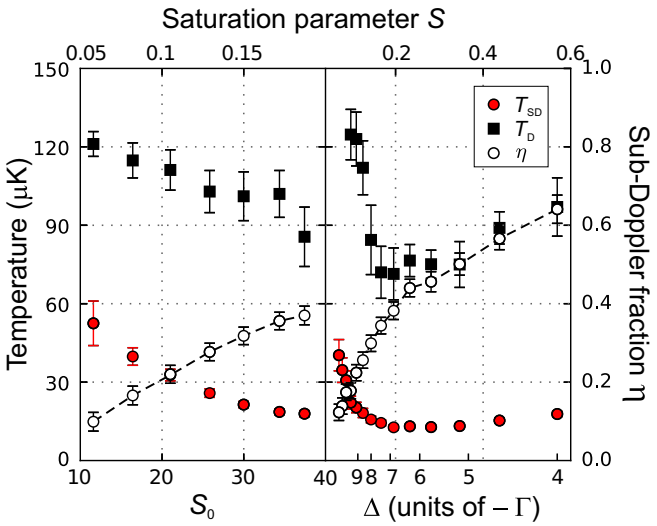

FIG. 4. Temperature of the Doppler T_D (black squares) and the sub-Doppler T_{SD}(red circles) subensembles depending on the light intensity and frequency detuning. Open circles show the fraction η of the sub-Doppler cooled atoms. Left plot: Intensity I ($S_0 \propto I$) is changed at fixed $\Delta = -7\Gamma$. Right: Light detuning Δ is changed at fixed $I = 11.8\,\mathrm{mW/cm^2}$ ($S_0 = 37$). In both experiments the magnetic field gradient equals $b = 0.07\,\mathrm{T/m}$. Top axes show the corresponding saturation parameter S.

One should note that MOT regimes smoothly transform from one to another without clear boundaries. Nevertheless, theoretical estimates for S_{b1} and S_{b2} show reasonable agreement with our experimental observations.

For comparison, let us consider Tm first-stage cooling at the spectrally broad transition (410.6 nm). The corresponding boundaries will be $S_{b1} = 5 \times 10^{-5}$ and $S_{b2} = 7 \times 10^{-4}$ (comparable to the values for a ^{87}Rb MOT [29] of $S_{b1} = 9 \times 10^{-5}$ and $S_{b2} = 6 \times 10^{-4}$). For a typical first-stage Tm MOT [20], we use $S_0 \approx 0.1$ and $\Delta \approx -\Gamma$, which correspond to the case $S = 0.02 \gg S_{b2}$. In this case the width of the polarization-gradient resonance is large enough to play a dominant role in the cooling process, resulting in a regular one-temperature Maxwellian distribution of atoms [Fig. 2(d)]. For much smaller saturation parameters the number of trapped atoms rapidly decreases [15], making observation of other MOT regimes difficult.

Double structures were previously reported for Rb [30], Dy [21], and Ca [31] MOTs. The specific cloud density profile in the Rb MOT was caused by a biharmonical confining potential coming from the sub-Doppler part of a magneto-optical trapping force [30]. For the Dy and Ca MOTs the double structure comes directly from the two-component Maxwellian momentum distribution, which resembles our case. The Dy MOT operates at the broad transition ($\Gamma = 2\pi \times 32\,\mathrm{MHz}$) and the two-temperature distribution appears only due to the influence of the magnetic field on the cooling process. The Ca MOT works at the narrow transition ($\Gamma = 2\pi \times 57\,\mathrm{kHz}$) involving atoms in a metastable state. As a result the atomic cloud doesn't attain thermal equilibrium, which results in a non-Maxwellian momentum distribution. The double-structured MOT of the same origin as in our case was predicted for Mg atoms cooled on the $3^3P_2 \rightarrow 3^2D_3$ transition [32,33].

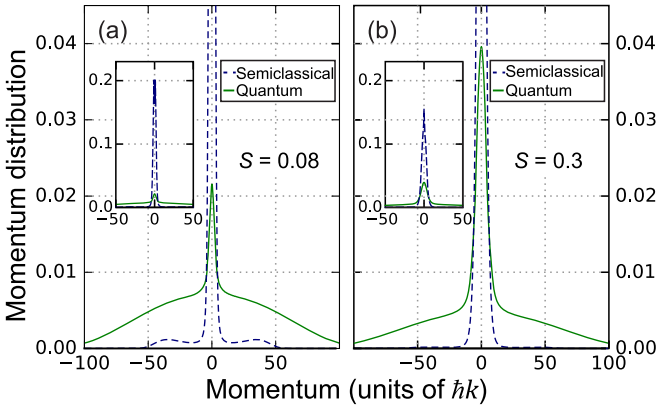

FIG. 5. Stationary momentum distribution of Tm atoms in the one-dimensional σ^+-σ^- optical molasses, showing a comparison of the semiclassical calculations (blue dashed line) and full quantum treatment (green solid line).The insets show full scale views. Calculations are performed for (a) $S = 0.08$ ($I = 5\,\mathrm{mW/cm^2}$, $\Delta = -7\Gamma$) and (b) $S = 0.3$ ($I = 20\,\mathrm{mW/cm^2}$, $\Delta = -7\Gamma$).

III. SEMICLASSICAL AND QUANTUM DESCRIPTIONS OF THE DOUBLE-STRUCTURE REGIME

A. Semiclassical approach, molasses

To analyze in detail the double-structure regime, we performed numerical simulations of the cooling process. First, we tried to reproduce the observed momentum distribution using the semiclassical model of one-dimensional optical molasses in the σ^+-σ^- configuration at zero magnetic field [23]. The calculation was performed at the detuning $\Delta = -7\Gamma$ for intensities of 5 $\mathrm{mW/cm^2}$ ($S_0 = 15.6$, $S = 0.08$) and 20 $\mathrm{mW/cm^2}$ ($S_0 = 62.5$, $S = 0.3$). Results of the calculation are shown in Fig. 5 with dashed lines.

As expected, the atomic momentum distribution consists of a narrow peak around zero momentum representing a cold atomic fraction and a wide pedestal corresponding to a hot fraction of atoms. We find that momentum profile of the hot fraction strongly deviates from a Gaussian [Fig. 5(a)]. Also, the relative number of hot atoms (pedestal area) rapidly decreases for the higher saturation parameter and is below 5% at $S = 0.3$ [Fig. 5(b)]. Both of these results contradict experimental observations which means that the semiclassical treatment is not valid in our case.

B. Quantum approach, molasses

As an alternative approach, we used the full quantum treatment described previously in Refs. [24,25]. In contrast to the semiclassical case, this approach takes fully into account the recoil effect. We numerically solve the master equation for atomic density matrix which gives full information of the system. As in the previous case, calculations are performed for the one-dimensional configuration in the absence of magnetic fields. Results of the simulations are shown in Fig. 5 together with the semiclassical ones. One can see that the quantum treatment also predicts a significantly non-Maxwellian momentum distribution consisting of two distinct subensembles. There is a cold fraction accumulated around zero momentum and a wide pedestal spreading up to $\pm 100\hbar k$.

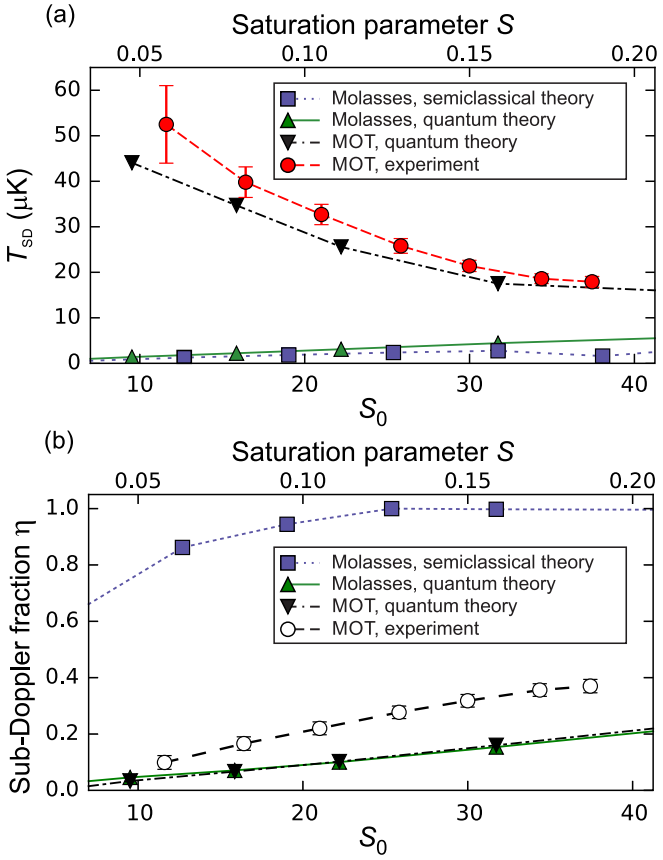

FIG. 6. (a) Temperature of the sub-Doppler cooled atoms T_{SD} and (b) the sub-Doppler fraction η_{cold} depending on the cooling light intensity I ($S_0 \propto I$). We show results of the semiclassical approach for molasses (blue squares), the quantum approach for molasses (green upward triangles), and the quantum approach with the MOT magnetic field taken into account (black downward triangles). Experimental results for T_{SD} (red circles) and η_{cold} (white circles) are taken from Fig. 4. The magnetic field gradient equals $b = 0.07$ T/m, and the detuning is $\Delta = -7\Gamma$.

Despite qualitative similarity, the results of the quantum and the semiclassical approaches strongly differ mainly by the shape and the weight of the pedestal. The momentum distribution obtained by the quantum approach can be well approximated by two independent Gaussian functions, one for the central peak (cold atomic fraction) and one for the pedestal (hot fraction). It allows us to deduce individual temperatures of two subensembles T_{SD} and T_D as well as the fraction η of the sub-Doppler cooled atoms, similar to the experimental case (Sec. II).

A comparison of the two theoretical approaches (semiclassical and quantum) with the experiment is presented in Fig. 6. The results of quantum theory ("molasses, quantum theory") and semiclassical theory ("molasses, semiclassical theory") give similar prediction for the temperature of the sub-Doppler cooled atoms T_{SD} in the range 0.5–5 μK, which grows with the saturation parameter S. Both theories predict much lower temperatures (1–5 μK) compared to what have been observed in the experiment (20–50 μK).

C. Quantum approach, MOT

Along with the recoil effect, one has to account for the magnetic field of the MOT. Indeed, the magnetic field can be neglected only if the Zeeman splitting of the ground state $\Delta E/\hbar$ is much smaller compared to the spectral width of the sub-Doppler resonance ΓS [34]:

$$\Delta E/\hbar = \mu_B g_F B/\hbar \ll \Gamma S, \tag{5}$$

where μ_B is the Bohr magneton, g_F is the Landé g factor of the ground state and B is the magnetic field. In our experiment, $S \sim 0.1$ and the magnetic field gradient equals $b = 0.07$ T/m, so the magnetic field can be neglected only in a small area of 10 μm around the trap center. A typical cloud size of the Tm MOT is about 100 μm which means that the magnetic field significantly impacts the cooling process by decreasing the polarization-gradient cooling efficiency.

To take into account the influence of the magnetic field we applied the density matrix method previously developed in [24,25] with an assumption that the motion of the atoms in the MOT is much slower compared to the cooling rate. Indeed, for our range of parameters the MOT oscillation frequency is close to 1 kHz, while the recoil frequency, describing the cooling rate ($\tau_{cool} \sim \omega_{rec}^{-1}$) is $\omega_{rec}/2\pi = \hbar k^2/4\pi m = 4.2$ kHz. Thus, we can assume adiabatic motion of the atoms in the magneto-optical potential with the equilibrium momentum distribution determined by the local magnetic field at the position z. This assumption allows us to derive the total momentum distribution of our atomic ensemble by averaging partial contributions from distinct subensembles distributed along the z axis.

Simulations show that the magnetic field significantly modifies the temperature and spatial distribution of the cold sub-Doppler fraction of atoms. The temperature T_{SD} calculated in the presence of the magnetic field is shown in Fig. 6(a) as "MOT, quantum theory." In the presence of the magnetic field the temperature grows up to one order of magnitude indicating that the polarization-gradient cooling becomes less efficient. Also, the slope changes sign: now T_{SD} decreases at higher intensities I. As one can see from Fig. 6(a), results of the calculations in the presence of a magnetic field reproduce our experimental observations well.

The specific behavior of $T_{SD}(S_0)$ can be qualitatively explained by the following. At higher intensities I, the width of the sub-Doppler resonance becomes larger and the criterion Eq. (5) becomes valid for a larger volume. As a result, the efficiency of the sub-Doppler cooling increases, and the momentum distribution approaches the one predicted by the molasses theory.

As shown in Fig. 6(b), the fraction of the sub-Doppler cooled atoms η predicted by the quantum theory is significantly smaller than the semiclassical one. Taking the magnetic field into account generally does not impact this fraction, so the results for the molasses and for the MOT nearly coincide. We see that the experimental results again are much better reproduced by the quantum approach rather than by the semiclassical one. The remaining discrepancy can be explained by the fact that simulations take into account the whole initial atomic ensemble, while in the experiment the hottest atoms cannot be trapped in the finite MOT potential.

The latter also explains the significant discrepancy between the temperature T_D deduced from the simulations (typically about 1 mK) and from the experiment (100 μK). Indeed, the loss of the fastest atoms results in a significant change of temperature and makes the corresponding comparison uninformative.

Thus, using the quantum theory for a one-dimensional atomic gas in the presence of a magnetic field, we adequately reproduced competitive processes between the Doppler and the sub-Doppler cooling mechanisms taking place in the second-stage Tm MOT operating at 530.7 nm.

To the best of our knowledge, one-dimensional models of the MOT give the same result as three-dimensional models at the low saturation limit [35–37]. Because of this, we restrict our calculations to the one-dimensional case for simplicity.

IV. CONCLUSION

We experimentally study the second-stage Tm MOT operating at the 530.7 nm transition with an intermediate spectral linewidth of 350 kHz. This gives an interesting opportunity to observe three distinct MOT regimes depending on the saturation parameter S. The most intriguing regime can be observed for S ranging from 0.05 to 0.5 when the cloud consists of the sub-Doppler and the Doppler cooled fractions. Both processes compete depending on the saturation parameter S with the sub-Doppler cooled fraction increasing at higher S.

We expand the previously reported one-dimensional full-quantum treatment by taking the MOT magnetic field into account to numerically calculate velocity distribution of atoms in the MOT. We show that this model reproduces the experimental data well and can be successfully applied to describe kinetics of atoms in the MOT.

ACKNOWLEDGMENTS

The authors acknowledge support from RFBR Grants No. 15-02-05324 and No. 16-29-11723. The research work of O.N.P. was supported by RSF (Project No. 16-12-00054).

[1] J. J. McClelland and J. L. Hanssen, Phys. Rev. Lett. **96**, 143005 (2006).
[2] J. L. Bohn and D. S. Jin, Phys. Rev. A **89**, 022702 (2014).
[3] M. Lu, N. Q. Burdick, S. H. Youn, and B. L. Lev, Phys. Rev. Lett. **107**, 190401 (2011).
[4] A. Frisch, K. Aikawa, M. Mark, A. Rietzler, J. Schindler, E. Zupanič, R. Grimm, and F. Ferlaino, Phys. Rev. A **85**, 051401 (2012).
[5] G. A. Vishnyakova, E. S. Kalganova, D. D. Sukachev, S. A. Fedorov, A. V. Sokolov, A. V. Akimov, N. N. Kolachevsky, and V. N. Sorokin, Laser Phys. **24**, 074018 (2014).
[6] G. A. Vishnyakova, A. A. Golovizin, E. S. Kalganova, V. N. Sorokin, D. D. Sukachev, D. O. Tregubov, K. Y. Khabarova, and N. N. Kolachevsky, Usp. Fiz. Nauk **186**, 176 (2016).
[7] J. Miao, J. Hostetter, G. Stratis, and M. Saffman, Phys. Rev. A **89**, 041401 (2014).
[8] T. Lahaye, J. Metz, B. Fröhlich, T. Koch, M. Meister, A. Griesmaier, T. Pfau, H. Saito, Y. Kawaguchi, and M. Ueda, Phys. Rev. Lett. **101**, 080401 (2008).
[9] K. Aikawa, S. Baier, A. Frisch, M. Mark, C. Ravensbergen, and F. Ferlaino, Science **345**, 1484 (2014).
[10] T. Maier, H. Kadau, M. Schmitt, M. Wenzel, I. Ferrier-Barbut, T. Pfau, A. Frisch, S. Baier, K. Aikawa, L. Chomaz, M. J. Mark, F. Ferlaino, C. Makrides, E. Tiesinga, A. Petrov, and S. Kotochigova, Phys. Rev. X **5**, 041029 (2015).
[11] S. Baier, M. J. Mark, D. Petter, K. Aikawa, L. Chomaz, Z. Cai, M. Baranov, P. Zoller, and F. Ferlaino, Science **352**, 201 (2016).
[12] D. Sukachev, S. Fedorov, I. Tolstikhina, D. Tregubov, E. Kalganova, G. Vishnyakova, A. Golovizin, N. Kolachevsky, K. Khabarova, and V. Sorokin, Phys. Rev. A **94**, 022512 (2016).
[13] A. Kozlov, V. A. Dzuba, and V. V. Flambaum, Phys. Rev. A **88**, 032509 (2013).
[14] S. H. Youn, M. Lu, U. Ray, and B. L. Lev, Phys. Rev. A **82**, 043425 (2010).
[15] D. Sukachev, A. Sokolov, K. Chebakov, A. Akimov, S. Kanorsky, N. Kolachevsky, and V. Sorokin, Phys. Rev. A **82**, 011405 (2010).
[16] T. H. Loftus, T. Ido, A. D. Ludlow, M. M. Boyd, and J. Ye, Phys. Rev. Lett. **93**, 073003 (2004).
[17] A. J. Berglund, J. L. Hanssen, and J. J. McClelland, Phys. Rev. Lett. **100**, 113002 (2008).
[18] W. C. Martin, R. Zalubas, and L. Hagan, *Atomic Energy Levels - The Rare-Earth Elements*, Natl. Stand. Ref. Data Ser., Natl. Bur. Stand. (US) 60 (National Bureau of Standards, US Department of Commerce, Washington, 1978).
[19] G. Nave and U. Griesmann, Phys. Scr. **62**, 463 (2000).
[20] D. Sukachev, A. Sokolov, K. Chebakov, A. Akimov, N. Kolachevsky, and V. Sorokin, JETP Lett. **92**, 703 (2010).
[21] S. H. Youn, M. Lu, and B. L. Lev, Phys. Rev. A **82**, 043403 (2010).
[22] A. J. Berglund, S. A. Lee, and J. J. McClelland, Phys. Rev. A **76**, 053418 (2007).
[23] J. Dalibard and C. Cohen-Tannoudji, J. Opt. Soc. Am. B **6**, 2023 (1989).
[24] O. N. Prudnikov, A. V. Taĭchenachev, A. M. Tumaĭkin, and V. I. Yudin, J. Exp. Theor. Phys. **104**, 839 (2007).
[25] O. N. Prudnikov, R. Y. Il'enkov, A. V. Taichenachev, A. M. Tumaikin, and V. I. Yudin, J. Exp. Theor. Phys. **112**, 939 (2011).
[26] P. D. Lett, W. D. Phillips, S. L. Rolston, C. E. Tanner, R. N. Watts, and C. I. Westbrook, J. Opt. Soc. Am. B **6**, 2084 (1989).
[27] D. Dreon, L. A. Sidorenkov, C. Bouazza, W. Maineult, J. Dalibard, and S. Nascimbene, J. Phys. B: At. Mol. Opt. Phys. **50**, 065005 (2017).
[28] T. H. Loftus, T. Ido, M. M. Boyd, A. D. Ludlow, and J. Ye, Phys. Rev. A **70**, 063413 (2004).
[29] D. A. Steck, Rubidium 87 D line data, http://steck.us/alkalidata (revision 2.1.5, 13 January 2015).
[30] K. Kim, H.-R. Noh, H.-J. Ha, and W. Jhe, Phys. Rev. A **69**, 033406 (2004).

[31] D. P. Hansen, J. R. Mohr, and A. Hemmerich, Phys. Rev. A **67**, 021401 (2003).
[32] O. N. Prudnikov, D. V. Brazhnikov, A. V. Taichenachev, V. I. Yudin, A. E. Bonert, M. A. Tropnikov, and A. N. Goncharov, Laser Phys. **26**, 095503 (2016).
[33] O. N. Prudnikov, D. V. Brazhnikov, A. V. Taichenachev, V. I. Yudin, and A. N. Goncharov, Quantum Electron. **46**, 661 (2016).
[34] S.-Q. Shang, B. Sheehy, P. van der Straten, and H. Metcalf, Phys. Rev. Lett. **65**, 317 (1990).
[35] M. Gajda and J. Mostowski, Phys. Rev. A **49**, 4864 (1994).
[36] S.-K. Choi, S. E. Park, J. Chen, and V. G. Minogin, Phys. Rev. A **77**, 015405 (2008).
[37] O. N. Prudnikov, A. V. Taichenachev, and V. I. Yudin, J. Exp. Theor. Phys. **120**, 587 (2015).